Chaos and stability in a two-parameter family of convex billiard tables

Péter Bálint[1], Miklós Halász[1], Jorge A. Hernández-Tahuilán[2]‡ and David P. Sanders[2]

[1] Institute of Mathematics, the Budapest University of Technology and Economics, Egry József u. 1, H-1111, Budapest, Hungary

E-mail: pet@math.bme.hu , miklos.halasz@yahoo.co.uk

[2] Departamento de Física, Facultad de Ciencias, Universidad Nacional Autónoma de México, Ciudad Universitaria, 04510 México D.F., Mexico

E-mail: dps@fciencias.unam.mx

Abstract. We study, by numerical simulations and semi-rigorous arguments, a two-parameter family of convex, two-dimensional billiard tables, generalizing the one-parameter class of oval billiards of Benettin–Strelcyn [1]. We observe interesting dynamical phenomena when the billiard tables are continuously deformed from the integrable circular billiard to different versions of completely-chaotic stadia. In particular, we conjecture that a new class of ergodic billiard tables is obtained in certain regions of the two-dimensional parameter space, when the billiards are close to skewed stadia. We provide heuristic arguments supporting this conjecture, and give numerical confirmation using the powerful method of Lyapunov-weighted dynamics.

AMS classification scheme numbers: Primary: 37D50; Secondary: 37A25, 37J40, 37M25

1. Introduction

Billiard models are a class of Hamiltonian dynamical systems which exhibit the full range of behaviour from completely integrable to completely chaotic dynamics [2]. They consist of a point particle which collides elastically with the walls of a bounded region, the *billiard table*; the shape of the table determines the type of dynamics which is observed.

Several classes of two-dimensional billiard tables have been studied which interpolate between completely integrable and completely chaotic dynamics, including both one-parameter [1, 3, 4, 5, 6] and two-parameter [7] families. These allow us to observe the transitions by which the typical phase space, which is a mixture of ergodic, chaotic components, and regular KAM islands, evolves from one extreme behaviour to the other.

The chaotic limit is often represented by the Bunimovich stadium billiard, which consists of two semicircular arcs connected by two parallel line segments. When these two segments are non-parallel and one of the arcs is shorter, with the other being longer than a semicircle, we instead obtain the *skewed stadium* or *squash* billiard table. Such stadia are known to be ergodic and hyperbolic; however, as a consequence of so-called "quasi-integrable" phenomena, the hyperbolicity is non-uniform, and the dynamical behaviour is very sensitive to perturbations

‡ This paper is dedicated to the memory of Jorge Alejandro Hernández Tahuilán, who died tragically shortly after this paper was submitted. This work formed part of his Master's thesis, and was to be his first published article.

of the boundary. There is an abundance of literature on stadium billiards; some works that are relevant to our discussion are refs. [8, 9, 10, 11, 12]; see also section 2.1 for a more detailed description of stadia.

In this paper, we study a two-parameter set of two-dimensional billiard tables which generalizes the one-parameter family of oval billiards studied in refs. [1, 3] in a particular way; see section 2.2 for an explicit description. Our models constitute a subcase of a rather general class of billiards introduced, but not studied in detail, by Hayli and Dumont [13]. Our class is of particular interest since it includes as limiting cases an entire family of ergodic skewed stadium billiards. Here these are generalised by deforming the sides of the stadia to circular arcs.

As in previous works on billiards formed from piecewise smooth components [1, 3, 13, 14, 7, 15, 16, 17, 18], for a large set of parameter values, we find coexistence of stability islands and chaotic components in phase space. However, we also find numerically that billiards which are sufficiently close to the limiting skewed stadia appear to have *no* remaining stability islands – the phase space is completely filled by a single chaotic, ergodic component. This motivates us to conjecture a new class of ergodic billiard tables. Similar conjectures have been suggested for other billiard models of similar type – see, e.g., [7].

Our case is, however, different from previous studies in several respects. Firstly, the new class introduced in this paper, and conjectured (for an open set of parameter values) to be ergodic, consists of *convex* planar billiards. The issue of ergodicity versus KAM islands in convex billiards has been the focus of continued interest for several decades. On the one hand, Lazutkin's fundamental theorem [19], and its strengthening by Douady [20], show that a convex planar billiard with at least C^6 boundary cannot be ergodic, due to the existence of caustics near the boundary of the billiard. Furthermore, recent results by Bunimovich and Grigo [21, 22] show that elliptic islands arise in C^2 stadium-like billiards (billiard tables constructed from stadia by replacing the discontinuity of the curvature with a C^2-smoothening).

On the other hand, several classes of convex planar billiards (with some discontinuity points of the curvature) are proved to be ergodic (see section 2.1 for a partial list of references). A common feature of these examples is the *defocusing* mechanism, which requires that whenever a narrow beam of (initially) parallel rays completes a series of consecutive reflections on one of the smooth focusing components of the billiard boundary, it must pass through a conjugate point and become divergent before the next collision with the curved (non-flat) part of the boundary; see [2, 21] for a more detailed description.

Defocusing (in this sense) cannot take place in our examples: since all boundary components are curved, it would require that the discs which complete each circular arc be contained inside the billiard table, which is prevented by the construction. Hence the mechanism which produces the (conjectured) ergodic behaviour must be different. We are aware of two other examples of ergodic planar billiards with focusing boundary components where defocusing is violated [23, 24]; however, non-convexity of the billiard domain plays an important role in both cases. Similarly, numerical studies in [7, 25] suggest ergodicity only for certain *non*-convex domains.

Secondly, even though a rigorous proof is currently not available, we give, in addition to the simulated phase portraits, further evidence which strongly supports our conjecture. Heuristic arguments are provided in section 4, which rely on the similarity of the dynamics with those of skewed stadia, and on the explicit analysis of sliding trajectories. The absence of islands is then tested numerically by the powerful method of Lyapunov-weighted dynamics in section 5. Before these arguments are given, the two-parameter family of generalised squashes is defined in section 2, and some numerical results on the dependence of the dynamics on the

two geometrical parameters are presented in section 3.

2. The model

We begin by defining the class of generalised squash billiard models.

2.1. Convex billiard tables

Consider a convex, compact domain $Q \subset \mathbb{R}^2$ bounded by a closed, piecewise-smooth curve $\Gamma = \partial Q$. The motion of a point particle that travels along straight lines with constant speed in the interior of Q, and bounces off elastically (angle of reflection equals angle of incidence) when reaching the boundary Γ, is referred to as *billiard dynamics*.

We investigate these dynamics in discrete time, that is, from collision to collision. The phase space is then the cylinder $M = \Gamma \times [0, \pi]$, with $M \ni x = (k, \varphi)$, where the configurational coordinate is the arc length k along the boundary, which satisfies $0 \leq k < |\Gamma|$ and describes the point of the closed curve Γ at which the collision takes place, while the velocity coordinate $0 \leq \varphi \leq \pi$ describes the angle that the outgoing velocity makes with the (positively oriented) tangent line to Γ at the point k.

Given $x \in M$, the position and velocity at the next collision are uniquely determined, so that the billiard map $T : M \to M$ is well-defined (provided that the boundary of the table is C^1-smooth). It is usual to visualize M as a rectangular domain in the plane, and the consecutive points along a trajectory of T as points in this domain. T has a natural invariant measure μ, which is absolutely continuous with respect to Lebesgue measure on M, given by

$$d\mu = \text{const} \,.\, \sin\varphi \, \mathrm{d}k \, \mathrm{d}\varphi.$$

For further material on billiards in general we refer to the monographs [2, 26].

The billiard map may show a surprisingly wide variety of dynamical phenomena for different choices of the billiard table Γ. The best known case is the billiard in a circle: for this geometry the dynamics are *integrable*: the angle of incidence φ is an integral of motion, the values of which label the invariant curves [2].

If Γ is a C^{553}-smooth closed curve, then for trajectories in the vicinity of the boundary the dynamics resemble, to some extent, those of the circular billiard: Lazutkin showed that a positive measure set of the phase space in a neighborhood of the boundaries $\varphi = 0$ and $\varphi = \pi$ is foliated by invariant curves [19], and Douady later lowered the requirement to C^6-smooth boundaries [20].

However, if Γ has less smoothness, then the billiard can be completely chaotic and ergodic. The first examples of such billiard tables are the celebrated stadia:

- the *straight stadium* is formed by two identical semicircles, joined at their endpoints by two parallel lines along their common tangents;
- the *skewed stadium*, or squash table, is formed by two circular arcs of different radii $r < R$, joined at their endpoints by non-parallel straight lines along their common tangents.

Stadia were introduced and their chaotic character first studied by Bunimovich in his famous paper [8]. It is known that for these tables the billiard map T is completely hyperbolic, i.e. there is one strictly positive and one strictly negative Lyapunov exponent for μ-a.e. $x \in M$, and T is ergodic with respect to μ; see [10, 2, 27] for a detailed description of stadia.

Stadia have three important characteristic features:

- The table boundary Γ is only *piecewise* smooth: at the intersection points of the circular arcs and straight lines, the curvature of the boundary (the second derivative) is discontinuous. The resulting singularities play a crucial role in the dynamics of the billiard map, both for the stadia and for the tables investigated below.
- The map T has many periodic points, all of which are either hyperbolic or parabolic. In the case of the circular billiard, all periodic points are parabolic. We will see below that in the generalised squash tables, the third class, elliptic periodic points, may also arise, typically giving rise to KAM islands in their vicinity.
- The billiard map T in stadia is only *non-uniformly* hyperbolic. The reason for this is the presence of so-called quasi-integrable – sliding, bouncing and diametrical – trajectory segments of arbitrary length (see figure 8). When the geometry is perturbed, these quasi-integrable phenomena may (or may not) create islands of integrability.

The mechanism that is responsible for the chaotic behaviour in stadium-shaped tables, known as the *defocusing mechanism*, has also been observed and studied in other classes of billiard tables in works of Bunimovich, Donnay, Markarian, Szász and Wojtkowski [28, 29, 30, 31, 32, 33]. However, the geometry of the billiards studied in this paper is quite different from the geometry of any of these classes.

2.2. The two-parameter family of generalised squashes

The family of convex billiard tables studied in this paper is described by two parameters, b and c. The table is built on a trapezium, whose geometry is specified by the parameter $0 \leq b \leq 1$. On each side of the trapezium is placed a circular arc joining its end-points, with adjacent arcs constrained to meet with common tangents; the parameter $1 \leq c \leq \infty$ specifies the ratio of the radii of the arcs.

More precisely, the base and the two sides of the trapezium are fixed to have unit length, and b is the length of the top, which is parallel to the base. The two extreme cases $b = 0$ and $b = 1$ correspond to the equilateral triangle and the square, respectively; see figure 1(a).

The table is left–right symmetric, with the circular arcs on the two sides having the same radius. The radii of the arcs on the base, sides and top are denoted R, R_∞ and r, respectively. As adjacent arcs are required to have a common tangent line where they meet, the shape of the table is determined by the value of any one of the radii – for a given trapezium (value of b), the geometry is parametrized by a single quantity, chosen for convenience to be the ratio $c := R_\infty/R$; see figure 1. For brevity, throughout the paper the arcs corresponding to the base, the sides and the top are referred to as the bottom arc, the "almost-flat" arcs, and the top arc, respectively. The construction of the tables is detailed in the Appendix; they can be viewed as a subfamily of a general class of billiards introduced in [13].

The case $c = 1$ gives a circle for any value of b; the case $b = 1$ and $c = \infty$ corresponds to the straight stadium; and the case $b < 1$ and $c = \infty$ gives a skewed stadium, with the amount of skewness depending on the value of b. Thus, by changing c, we may continuously deform the integrable dynamics of the circular billiard into a completely-chaotic billiard.

The transition for the case $b = 1$ (oval billiards based on a square) has previously been studied [1, 3], although with a different parametrisation. In this paper, we concentrate instead on the role of the parameter b, which determines the relative width of the top and bottom sections of the billiard, and which leads to distinct phenomena for finite, but large enough, c. We remark that an important role is played by so-called "quasi-integrable" phenomena, which are common to all stadium-type billiards. These consist in arbitrarily long sequences of collisions which do not contribute to hyperbolic behaviour; details are given in section 4.

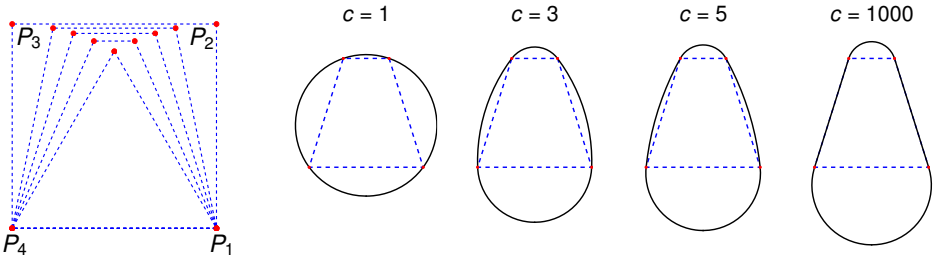

(a) Trapezia for $b = 0$, 0.2, 0.4, 0.6 and 1.0 (inside to outside).

(b) Effect of the parameter c, with $b = 0.4$ fixed.

Figure 1. Variation of the geometry of the generalised squash billiards as a function of the two parameters b and c.

3. Parameter-dependence of dynamics

In this section, we survey the types of dynamical behaviour observed in numerical experiments in the two-dimensional (b,c) parameter space. The numerical methods used are briefly described in the Appendix. Numerical results for other billiard models formed by piecewise-smooth curves can be found in refs. [1, 3, 13, 14, 7, 15, 16, 17, 18].

3.1. Parameter space

It is useful to start from the known behaviour of the oval billiards obtained when $b = 1$ [1, 3]. In this case, when $c = \infty$, the table is an ergodic straight stadium. As soon as c is decreased to a finite value, however, ergodicity of the billiard map is ruined. More precisely, *elliptic islands* – regions of positive Lebesgue measure which are foliated by invariant curves and concentrated around elliptic periodic points – appear in the phase space. For $c > 1$, coexistence of such elliptic islands and ergodic components of positive measure ("chaotic sea") is observed. For large enough c, there is a single chaotic component (still coexisting with elliptic islands), while the number of chaotic components increases once c is decreased below certain thresholds. The references [1, 3] concentrate on this phenomenon of splitting of chaotic components.

The phenomenology is initially similar when we introduce $b < 1$. For c close to the limiting integrable case $c = 1$, the phase space is dominated by elliptic islands. For $c \gtrsim 1.2$ it is already possible to observe a finite number of ergodic components, each of positive Lebesgue measure ("chaotic seas") which fill most of the phase space, while for $c \gtrsim 1.5$ we observe a single, dominant ergodic component. The splitting of ergodic components studied in refs. [1, 3] occurs at $c \simeq 1.35$ when $b = 1$, while for $b < 1$ we observe similar phenomena, but restricted to a smaller range of c.

As we increase c further, the proportion of phase space occupied by elliptic islands has a tendency to decrease, and beyond a certain threshold, no remaining islands are numerically observed. This leads to our main conjecture (section 3.4) that the system is ergodic in a certain region of parameter space.

3.2. Existence and stability regions of periodic orbits

Elliptic islands are concentrated around elliptic periodic orbits, so studying the existence and stability properties of such orbits is critical [7]. For the $b = 1$ case, an important feature of

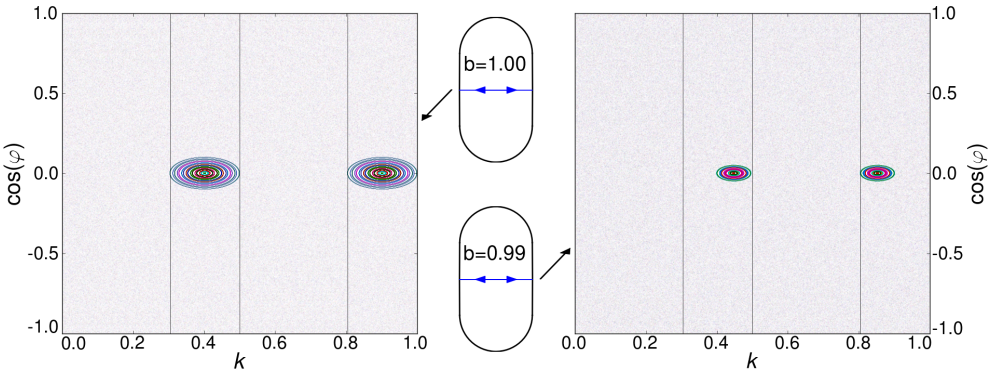

Figure 2. The period-2 orbit and corresponding island in phase space for $c = 100$ with $b = 1$ (left) and $b = 0.99$ (right).

the dynamics is a period-2 orbit which is present for *any* finite value of c, and which bounces perpendicularly between the midpoints of the almost-flat arcs. Its stability properties – in particular, the stability parameter s (cf. Appendix B) – can easily be calculated: when $c < \infty$ (that is, $R_\infty < \infty$), it is elliptic, and gives rise to an island. As shown in figure 2(a), the island around this orbit extends across the whole range of k along the almost-flat arcs, while its width in the φ direction decreases as c is increased.

For $b < 1$, however, the width of the island shrinks both in the k and in the φ directions as c is increased, as shown in figure 2(b), and finally *disappears* for large enough c. The reason is that the almost-flat arcs are now placed along two *non-parallel* sides of the trapezium, so that for large enough c there no longer exist points on these two arcs with mutually parallel tangent lines, and hence there is no such period-2 orbit. In this case, the bottom arc is forced to be longer than a semi-circle, due to the orientation of the tangent lines at the points where the bottom and almost-flat arcs join. The limit of existence of this period-2 orbit is thus when the bottom arc is exactly a semi-circle, which occurs at $c = c_0(b) := \frac{2}{1-b}$.

For $c > c_0(b)$, the period-2 orbit and its corresponding island disappear, but other islands, corresponding to periodic orbits of higher periods, appear in certain regions of the (b,c) plane. These islands generally appear in a certain window of values of c for a given, fixed b. Such stability regions for certain orbits of low period are shown in figure 3. For example, in the (blue) B region in the parameter space of figure 3, there exists an island around the period-4 orbit shown at the top right, for which the bounces on the bottom and left arcs are perpendicular (see also figure 4(a)).

3.3. Geometric destruction and period doubling of periodic orbits

A detailed study of the bifurcations occurring in the system is beyond the scope of this paper, and not our main goal here; instead, we give a short description of the main features that we have observed (see also [7]). We remark that bifurcation phenomena in piecewise-smooth systems are currently the subject of intensive studies – see e.g. [34, 35] and references therein.

Based on our observations, there are two kinds of dynamical phenomena that mainly determine whether an island of stability is formed around a periodic orbit. Firstly, the singularities of the boundary play an important role, since they influence the very existence of periodic orbits. To categorise such orbits, we use a coding of four symbols $\{B,R,T,L\}$, denoting bounces on the bottom, right, top and left arcs, respectively, and describe periodic

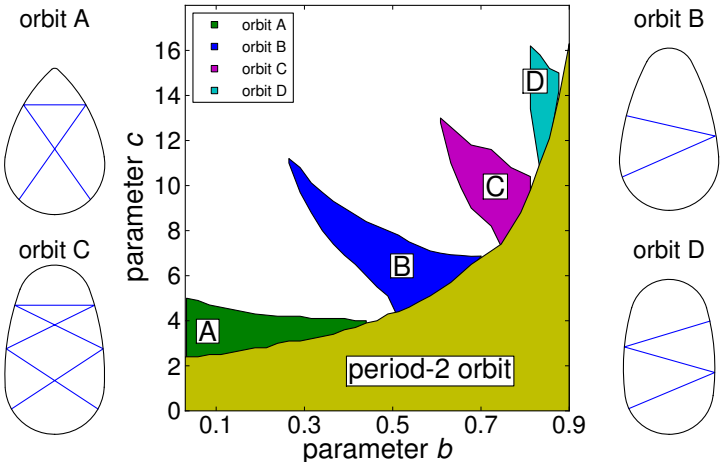

Figure 3. Regions of stability of certain types of periodic orbit. Each shaded region depicts the numerically-determined region of parameter space in which the corresponding labelled orbit type (with the same topology, or coding) is stable.

orbits according to a finite code (in general non-unique) of length equal to the orbit's period.

For example, consider again the period-2 orbit with code (R,L), which consists of consecutive perpendicular bounces on the two almost-flat arcs, and which exists for $c < c_0(b)$. As c tends to $c_0(b)$ from below, the locations of the collision points on the sides move closer to the ends of the almost-flat arcs, finally reaching the lower corner points (singularities) when $c = c_0(b)$. For larger values of c, this period-2 orbit with code (R,L) ceases to exist, since there are no points on the almost-flat arcs with mutually parallel tangent lines. We refer to this as *geometric destruction* of the periodic orbit.

However, geometric destruction is not the only mechanism by which an island corresponding to a periodic orbit may disappear. For example, figure 4(a) shows a period-4 orbit, around which an island of stability exists in the range $6.7 \lesssim c \lesssim 8.7$ for $b = 0.4$. When $c \simeq 8.7$, the orbit loses stability, even though its collision points are still located far from the singularities. In this case, the disappearance of the island is rather related to the stability properties of the periodic orbit.

In the setting of *smooth* dynamical systems, it is known that when a periodic orbit loses stability (the stability parameter $|s|$ increases above 2, cf. Appendix B), *period-doubling bifurcations* may be observed; see eg. [36]. As observed in [7], this can also occur in billiards, provided the periodic orbit stays away from the singularities.

Consider again the period-4 orbit studied above for $b = 0.4$. As c increases from $c \simeq 6.7$ to $c \simeq 8.7$, the stability parameter s decreases from 2 to -2; see figure 6. When c reaches the critical value 8.7, the shape of the island changes and it splits into two components, the centers of which are consecutive points of a period-8 orbit, shown in figure 4(b). The changes in shape of the corresponding islands which surround the periodic orbits is shown in figure 5. The period-4 orbit indeed undergoes a period-doubling bifurcation, becoming hyperbolic and giving rise to an elliptic period-8 orbit, around which the island forms. As c is increased further, the geometry of the period-8 orbit is deformed, and soon a collision point reaches a corner, resulting in geometric destruction of the island.

Similar period-doubling bifurcations occur for other periodic orbits when their disappearance is not due to geometric destruction. However, the presence of the singularities

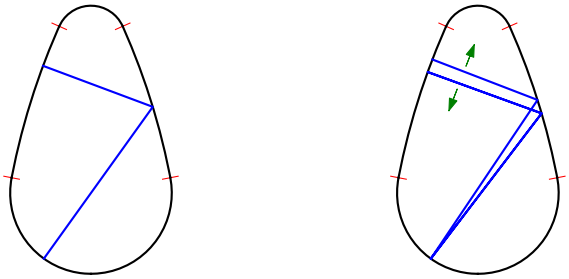

(a) Period-4 orbit with $c = 8.59$. (b) Period-8 orbit with $c = 8.61$.

Figure 4. Period-doubling bifurcation of a period-4 orbit for $b = 0.4$ as c is varied. The (red) thin straight lines indicate the singularities in the boundary of the squash, where the circular arcs are joined. The arrows indicate the direction in which the trajectory moves as c increases.

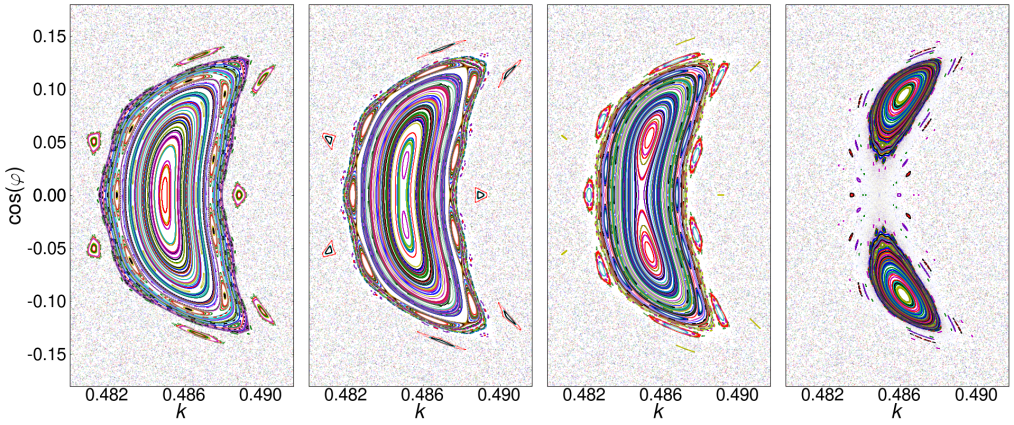

Figure 5. Phase-space structures for the period-doubling bifurcation of the elliptic periodic orbit shown in figure 4(a), highlighting the splitting of the corresponding island. Parameter values $b = 0.4$ and c = 8.59, 8.61, 8.63 and 8.69 from left to right.

modifies the picture significantly, so that islands are subject to the combination of two effects, geometric destruction caused by the singularities of the table, combined with the generic features characteristic of smooth systems with mixed phase space; see also [7, 37] for similar phenomena .

3.4. Main conjecture: a class of ergodic convex billiards

We now focus on the case of large c for some $b < 1$ fixed. The tendency is that as c increases, stability islands form around orbits of higher period. Typically, orbits of higher period are more sensitive to geometric destruction, since the presence of more bounces leads to more possibilities for one of the collision points to collide with a singularity when the parameters are varied. Thus the area in phase space of higher-period islands tends to decrease with increasing period. For this reason, the region in the parameter space where period-doubling

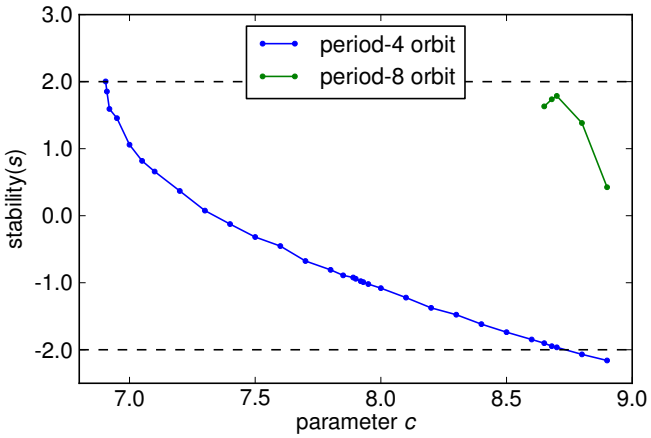

Figure 6. Dependence of the stability on c for the period-4 and period-8 orbits shown in figure 4.

bifurcation phenomena can actually be observed is quite limited.

Furthermore, as the parameter c is increased even further, it appears that *all* islands disappear, and that the system thus becomes ergodic. These numerical observations motivate the following conjecture:

Main conjecture. *For any $b < 1$, there exists $\hat{c}(b)$ such that for any pair of parameters (b,c) with $c > \hat{c}(b)$ the billiard dynamics are ergodic.*

That is, once the generalised squash billiards are close enough to skewed stadia, we conjecture that they are ergodic. There is an obvious lower bound $\hat{c}(b) \geq c_0(b)$ on the region of ergodicity in parameter space (cf. section 3.2); both quantities tend to ∞ as b tends to 1, i.e. in the limit of oval billiards, for which there is never ergodicity for $c < \infty$.

Similar conjectures have been made for certain regions of parameter space in other billiards with piecewise-smooth boundaries [7]. Here, however, we provide heuristic arguments, and confirmation using a more powerful numerical method, in the next two sections.

4. Heuristic support for the conjecture

In this section, we support our conjecture with heuristic arguments. Even though a rigorous proof, which appears to be a technically challenging task, is currently not available, we believe that we capture the key phenomena.

Our heuristic argument relies on a comparison of the dynamics of the model for large c with the limiting case $c = \infty$, i.e. the skewed stadia, which have been extensively studied We first summarize the key characteristics of the dynamical behavior of these stadia ($c = \infty$); for more details, see in particular refs. [10, 11, 38].

4.1. Dynamics of skewed stadia ($c = \infty$)

On a large part of phase space, the billiard dynamics for stadia is strongly hyperbolic. It is, on the other hand, possible to locate precisely the places where hyperbolicity can be

arbitrarily weak: these correspond to quasi-integrable (bouncing, diametrical or sliding) trajectory segments, which can be analysed by direct geometrical arguments. Roughly, if one considers a smooth curve in the phase space that has completed a quasi-integrable segment of length $n_1 \gg 1$, then the points along this curve will begin another quasi-integrable segment of length $n_2 \gg 1$, and, assuming that the curve is sufficiently stretched out, it is possible to calculate the transition probabilities for the allowed $n_1 \to n_2$ transitions. By this analysis one observes that, on the average, n_2 is smaller than n_1. This results in escaping from the quasi-integrable region: almost every point leaves this part of the phase space after a finite number of consecutive quasi-integrable segments.

The above behavior plays a crucial role in the analysis of stadia; it resulted, for example, in the proof of finer statistical properties like correlation decay rates and statistical limit laws [2, 10, 11] and in the investigation of survival probabilities [12]. As already mentioned above, a mathematically rigorous proof of our main conjecture is beyond the scope of the present paper. Instead, we argue that generalized squashes show a dynamical behavior very similar to the one sketched above. More precisely, on a large part of the phase space – in particular, apart from sliding trajectory segments – the dynamics for the $c = \infty$ and the finite $\bar{c} \gg 1$ cases are directly comparable. On the other hand, sliding trajectory segments can again be analysed by direct geometrical arguments, and we observe escape from the quasi-integrable region in the sense described above.

4.2. Notation and phase spaces

A key ingredient of our argument is the comparison of the billiard maps for $c = \infty$ and $\bar{c} \gg 1$, for the same value of $b < 1$. To compare the two maps, their phase spaces are identified by a map $\chi : M^{\bar{c}} \to M^{\infty}$, which is defined below. Throughout, upper indices refer to the value of c ($c = \infty$ or $\bar{c} \gg 1$ finite), which we omit if the description applies to both cases; later, we will also need to compare maps for different b, in which case the two upper indices (b,c) of the map will be given.

For $x = (k, \varphi) \in M$, with $0 \le \varphi \le \pi$ and $0 \le k < |\Gamma|$, let $0 = k_0 < k_1 < k_2 < k_3 < k_4 = |\Gamma|$ denote the arclength coordinates of the corner points separating consecutive arcs. We denote by M_B, M_R, M_T and M_L the sets of points (k, φ) with $k \in [k_0, k_1]$, $k \in [k_1, k_2]$, $k \in [k_2, k_3]$ and $k \in [k_3, k_4]$, respectively – that is, phase points on the bottom, right, top and left arcs. We also denote the angles of the bottom and top arcs by $2\alpha_B$ and $2\alpha_T$, respectively, so that $k_1 = 2R\alpha_B$ and $k_3 - k_2 = 2r\alpha_T$, where R and r are the radii of the bottom and top arcs, respectively. The set $\bar{M} = \bar{M}_B \cup \bar{M}_T$, where

$$\bar{M}_B = \left\{ (k,\varphi) \in M_B \,|\, (\pi - \alpha_B)\frac{k}{k_1} \le \varphi \le (\pi - \alpha_B)\frac{k}{k_1} + \alpha_B \right\};$$
$$\bar{M}_T = \left\{ (k,\varphi) \in M_T \,|\, (\pi - \alpha_T)\frac{k-k_2}{k_3-k_2} \le \varphi \le (\pi - \alpha_T)\frac{k-k_2}{k_3-k_2} + \alpha_T \right\},$$

a union of two parallelograms, plays a special role in our discussion. Note that $x \in \bar{M}$ if and only if x is on the bottom arc and its image, Tx, is not on the bottom arc, and a similar characterization applies to $\bar{M}_T$ with respect to the top arc. See Figure 7 for the geometry of the geometry of these sets. As $\bar{M}$ is of positive measure, the first return map $\bar{T} : \bar{M} \to \bar{M}$ is naturally defined, and for the case of $c = \infty$, $\bar{T}^{\infty} : \bar{M}^{\infty} \to \bar{M}^{\infty}$ is known to have strong hyperbolic properties – see eg. [10]. To exploit this fact, it is not so much the billiard maps $T^{\bar{c}}$ and T^{∞}, but rather the first return maps $\bar{T}^{\infty}$ and $\bar{T}^{\bar{c}}$, that we would like to compare.

This motivates the definition of the identification map $\chi : M^{\bar{c}} \to M^{\infty}$, as follows. Note that both $M_B \setminus \bar{M}_B$ and $M_T \setminus \bar{M}_T$ are unions of two triangles, hence the phase space M can

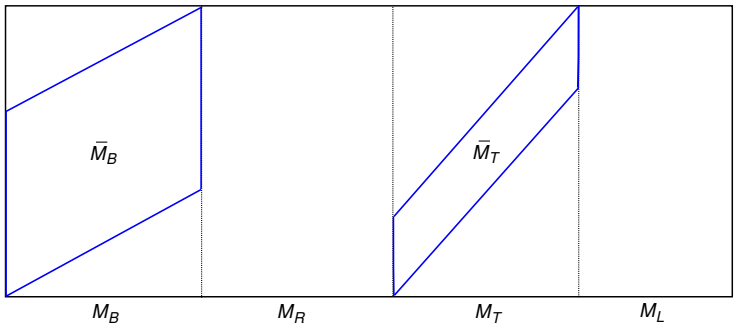

Figure 7. The sets $\bar{M}_B$ and $\bar{M}_T$. The phase space is partitioned into 8 pieces on each of which the identification map χ is linear.

be regarded as a union of 8 polygonal pieces – two rectangles, two parallelograms and four triangles; see figure 7. The map $\chi : M^{\bar{c}} \to M^{\infty}$ is piecewise linear: it rescales linearly each of the 8 polygonal pieces of $M^{\bar{c}}$ onto the corresponding polygonal pieces of M^{∞}. Note that χ matches the complete arcs of $M^{\bar{c}}$ with the complete arcs of M^{∞}, and it matches $\bar{M}^{\bar{c}}$ with $\bar{M}^{\infty}$. Furthermore, the singularity set of χ and χ^{-1} is contained in the singularity set of $T^{\bar{c}}$ and T^{∞}, respectively. These properties ensure that $\bar{T}^{\infty}$ and $\bar{T}^{\bar{c}}$ can be compared on a large part of $\bar{M}$, specified precisely below. It is also worth noting that the identification map can be defined if the values of b are not equal in the cases $c = \bar{c}$ and $c = \infty$.

4.3. First-return maps

To proceed, we recall the notion of symbolic collision sequence (or code) from section 3.3: the symbolic sequence for the trajectory segment $(x, Tx, ..., T^N x)$ is $A_N(x) = (a_0, a_1, ..., a_N)$, where $a_i \in \{B, R, T, L\}$ specifies the arc (bottom, left, top or right) on which $T^i x$ is located. Note that the tangent map DT_x^N at $x \in M$ is well-defined if and only if $A_N(x)$ is unique, that is, none of the points $T^i x$ $(i = 0, ..., N)$ collides exactly at a corner (in other words, T^N is not singular at x). If x is singular, i.e. $T^i x$ lies at the corner point of two consecutive arcs for some $i \in \{0, ..., N\}$, then a_i can take two possible values, hence several collision sequences, and, correspondingly, several tangent maps DT_x^N can be defined.

Now let us turn back to the investigation of the first-return map $\bar{T} : \bar{M} \to \bar{M}$. We recall an important property of the skewed stadium from [10]: $\bar{T}^{\infty}$ is *uniformly hyperbolic*, in the following sense; there exists some $\Lambda > 1$ and cone fields C_x^s, C_x^u (stable and unstable cones) in the tangent bundle of $\bar{M}^{\infty}$, such that

(i) for $v \in C_x^u$, we have $D\bar{T}_x^{\infty} v \in C_{\bar{T}^{\infty} x}^u$ and $|D\bar{T}_x^{\infty} v| > \Lambda |v|$; and

(ii) for $w \in C_{\bar{T}^{\infty} x}^s$, we have $(D\bar{T}_x^{\infty})^{-1} w \in C_x^s$ and $|(D\bar{T}_x^{\infty})^{-1} w| > \Lambda |w|$.

If $\bar{T}^{\infty}$ is singular at x (i.e. the trajectory of $x \in \bar{M}^{\infty}$ hits at least one corner before returning to $\bar{M}^{\infty}$), then properties (i) and (ii) above hold for the tangent map corresponding to any of its symbolic collision sequences.

Now, using the identification map χ, we argue that $\bar{T}^{\bar{c}}$ is also uniformly hyperbolic in the above sense, on a "large part" (specified below) of $\bar{M}^{\infty}$. First observe that the billiard tables for $c = \infty$ and $c = \bar{c}$ are piecewise C^2-close – that is, the bottom, right, top and left arcs for $c = \bar{c}$ are C^2-close to their $c = \infty$ counterparts, as curves in the plane. We recall some properties of the billiard map from [2]; see also formula (B.1) in the Appendix. C^2-closeness of the billiard tables would imply that the maps $T^{\bar{c}}$ and T^{∞} are C^1-close; however, the billiard map

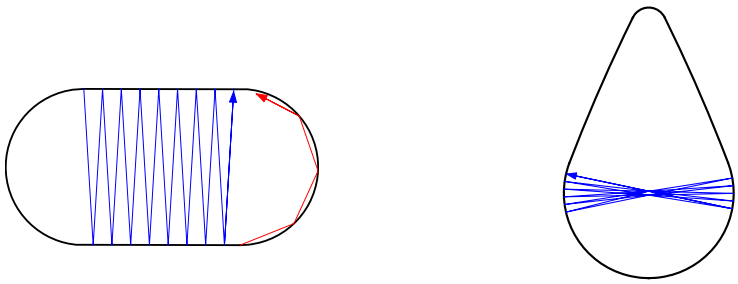

(a) Bouncing and sliding orbits. (b) Diametrical orbits.

Figure 8. Quasi-integrable phenomena present in stadia.

is only piecewise smooth and may have unbounded derivatives corresponding to tangential collisions. Thus, $T^{\bar{c}}$ and T^{∞} are C^1-close unless $\varphi \simeq 0$ or $\varphi \simeq \pi$, in the following sense. For any $\varepsilon > 0$ there exists $\bar{c}$ such that if $c > \bar{c}$, then given any $(k,\varphi) = x \in M_c$ with $\varepsilon < \varphi < \pi - \varepsilon$ and symbolic collision sequence (a_0, a_1), then there exists $x' \in M^{\infty}$ with the same collision sequence (a_0, a_1), for which $d(x', \chi(x)) < \varepsilon$ and $d(Tx', \chi(Tx)) < \varepsilon$, and the tangent maps DT^c_x and $DT^{\infty}_{x'}$ are ε-close. If x is singular, then it is possible to find such $x' \in M^{\infty}$ for both of its collision sequences.

We would like to conclude that (apart from tangencies) $\bar{T}^{\bar{c}}$ is also C^1-close to $\bar{T}^{\infty}$, and thus, $\bar{T}^{\bar{c}}$ is also uniformly hyperbolic (as uniform hyperbolicity is a C^1-open property). However, closeness of the T's implies closeness of the $\bar{T}$'s only if phase points $x \in \bar{M}$ are considered for which $\bar{T}x = T^{n(x)}x$, such that $n(x)$, the number of iterates needed to return to $\bar{M}$, is *uniformly bounded*. Thus, we need to consider the complement of this set: points with unbounded return time, which are exactly the points from which the quasi-integrable trajectory segments originate. At this point the differences between the $b < 1$ and $b = 1$ cases play an important role, as follows.

4.4. Quasi-integrable phenomena

For *bouncing points* $x = (k,\varphi) \in \bar{M}$ (see figure 8(a)), returns to $\bar{M}$ consist of a high number of consecutive collisions on the almost-flat arcs. If $b = 1$, then such orbits may spend an unbounded number of iterations bouncing close-to-perpendicularly on the almost-flat arcs. However, if $b < 1$, then the number of such bounces, and thus the time needed to return to $\bar{M}$, is uniformly bounded (the bound, of course, depends on the actual value of b, which affects the value of $\hat{c}(b)$ in Conjecture 3.4).

Diametrical quasi-integrable motion, when the trajectory bounces back and forth between two diametrically-opposite points of a circle (figure 8(b)) may also correspond to unbounded return time. This phenomenon is dominated by the bottom arc of the $b < 1$ case: returns to $\bar{M}$ consist of a diametrical trajectory segment (that can be arbitrarily long) and a single bounce on one of the almost-flat arcs (cf. [10]). This allows us to compare directly the derivatives of the return maps $\bar{T}^{\infty}$ and $\bar{T}^{\bar{c}}$ at such points. In fact, here it is more useful to compare the maps $\bar{T}^{b,\bar{c}}$ and $\bar{T}^{\bar{b},\infty}$ with different values of the parameter b, where $\bar{b} \simeq b$ is chosen in such a way that the bottom arc of the skewed stadium for $(\bar{b}, \infty)$ is identical to

the bottom arc of the generalized squash for $(b,\bar{c})$ (the two arcs have equal radii and equal lengths) – the identification map $\chi : \bar{M}^{b,\bar{c}} \to \bar{M}^{\bar{b},\infty}$ can be easily generalized to this case. The advantage of this choice is that now it is possible to find $x' \in \bar{M}^{\bar{b},\infty}$ close to $\chi(x)$ such that the diametrical trajectory segments of x and x' are identical.

To compare the tangent maps for x and x', we use the local orthogonal section (cf. Appendix B). Consider $x \in \bar{M}^{b,\bar{c}}$ with return time $n(x) = N+1$ performing diametrical quasi-integrable motion, and let us denote the derivatives of the return maps by $D_N := D_x(\bar{T}^{\bar{b},\infty})$ and $\bar{D}_N := D_{x'}(\bar{T}^{b,\bar{c}})$. Let us introduce, furthermore, the matrix B_N, the tangent map corresponding to N consecutive diametrical bounces on the bottom arc (our choice of $\bar{b}$ ensures that this part of the trajectory is identical in the two cases). Then $D_N = B_N \cdot A$ and $\bar{D}_N = B_N \cdot \bar{A}$, where the matrices A and $\bar{A}$ are the tangent maps corresponding to the single bounce on the flat arc of the $c = \infty$ case and on the almost-flat arc of the $c = \bar{c}$ case, respectively. We have the following results:

- D_N is strongly hyperbolic, and expands unstable vectors at least by a factor $k_1 \cdot N$ for some numerical constant $k_1 > 0$ (see ref. [10]).
- All elements of the matrix B_N have absolute value less than $k_2 \cdot N$ for some numerical constant $k_2 > 0$ (this can be easily checked by direct computation based on Formula (B.1)).
- Choosing $\bar{c}$ big enough, the difference of the matrices A and $\bar{A}$ can be made arbitrarily small: that is, for any $\varepsilon > 0$, there exists some finite c' such that whenever $\bar{c} > c'$, we have $||A - \bar{A}|| < \varepsilon$ (again from direct computation).

The above three facts imply that, choosing $\bar{c}$ big enough, $\bar{D}_N$ expands unstable vectors at least by a factor $k_3 \cdot N$ for some positive constant k_3. In particular, at points that give rise to diametrical motion, uniform hyperbolicity of the return map persists for finite, big enough $\bar{c}$.

4.5. Analysis of sliding trajectories

For the third type of quasi-integrable motion, *sliding points* (figure 8(a)), the $c = \infty$ and the finite $c = \bar{c} \gg 1$ cases cease to be comparable, hence these points need to be analysed directly for finite c. Note also that sliding can occur only if $\varphi \simeq 0$ or $\varphi \simeq \pi$.

The above arguments can be summarized as follows: fix the parameters (b,c) where $b < 1$ and $c > \hat{c}(b)$. Then there exists $\varphi_{b,c}$ such that $\bar{T}^{b,\bar{c}}$ is uniformly hyperbolic for any $x \in \bar{M}^{b,\bar{c}}$ for which $\varphi_{b,c} < \varphi < \pi - \varphi_{b,c}$. Furthermore, for any fixed $b < 1$, $\varphi_{b,c} \to 0$ as $c \to \infty$.

In other words, the dynamics is strongly chaotic unless φ or $\pi - \varphi$ is very small, that is, unless the trajectory "slides along the boundary" of phase space (see eg. refs. [10] or [8] for this terminology). Below, we give a direct geometrical description of the dynamics within this sliding region. This is a delicate issue, as it is exactly in this part of phase space where Lazutkin constructed caustics, and, correspondingly, a positive-measure set foliated by invariant curves. The crucial difference here from Lazutkin's setting is that the curvature of the boundary is discontinuous at the corner points which separate consecutive circular arcs. We will argue below that it is exactly these discontinuities that create "repulsion" from the sliding region.

In the rest of this section we fix $b < 1$ and $1 \ll c < \infty$, and omit upper indices. For concreteness, we describe the case when $\varphi \simeq 0$; the case when $\varphi \simeq \pi$ is completely analogous. In this region it is slightly more convenient to use, instead of the usual arclength k, the angular distance $\beta = k/R_{\text{arc}}$ along the arc of radius R_{arc}. Throughout, we will refer to the β coordinate as horizontal and the φ coordinate as vertical.

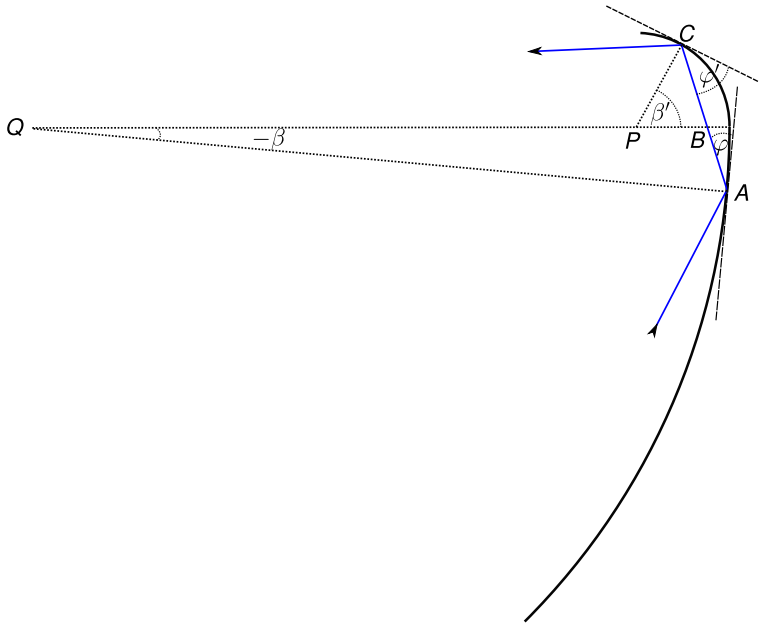

Figure 9. Geometry of switches between consecutive arcs.

Since φ is small, the trajectory experiences a long series of consecutive collisions on the same circular arc. Provided this happens, evolution in the coordinates (β,φ) is given by

$$(\beta',\varphi') := T(\beta,\varphi) := (\beta+2\varphi,\varphi); \tag{1}$$

in particular, φ is an integral of motion. Then, after some time, the trajectory bypasses a corner point and switches to the neighboring arc, followed by another long series of consecutive bounces on that arc. Thus there is an alternation of long series of sliding along the same arc and "switches" from one arc to another. Below we argue that as an overall effect of switching transitions, the value of φ increases, which means that the trajectory escapes from the sliding region.

More precisely, instead of a single phase point, we investigate the evolution of a one-parameter family of phase points. We will say that a curve is *good* if in the (β,φ) coordinates it has either nonnegative slope, or its slope is negative but bounded away from the horizontal direction (it is enough to require that either $\frac{d\varphi}{d\beta}\geq 0$, or $\frac{d\varphi}{d\beta}\leq -\frac{1}{2}$). We consider a family of phase points smoothly distributed along a good curve, and show that the value of φ increases strongly on the average when this family evolves under the dynamics. Before investigating switches a little closer, let us remark that the twist map (1) stretches curves in the horizontal direction: in particular, if a good curve is evolved by a high number of iterates of (1), then we get a curve of very small positive slope.

There are two types of transitions to be considered: switching from the bottom (or top) arc to an almost-flat arc, an $R\to R_\infty$ transition, or from an almost-flat arc to the bottom (or top) arc, an $R_\infty\to R$ transition. We first consider an $R_\infty\to R$ transition, and denote the coordinates by (β,φ) just before the transition (last bounce on the bottom/top arc) and $(\beta',\varphi')=T(\beta,\varphi)$ just after the transition (first bounce on the almost-flat arc). We normalize β such that $\beta=0$ corresponds to the corner point of the two arcs. Then $-2\varphi\leq\beta\leq 0$, and $0\leq\beta'\leq 2\varphi'$ (see figure 9 for a sketch of the geometry). It is also convenient to introduce $\omega=\beta+\varphi$ and

$\omega' = \beta' - \varphi'$. Note also that since the curve under consideration has experienced a long series of consecutive bounces on the almost-flat arc, its direction is close to horizontal, hence φ may be regarded as constant, and ω as evenly distributed on the interval $[-\varphi, \varphi]$. It is also apparent from figure 9 that the angles $QBA\sphericalangle$ and $PBC\sphericalangle$ sum up to π, hence $\omega' = \omega$. To express φ' in terms of φ and ω we use sine theorems for the triangles QAB and PBC on figure 9, giving

$$\frac{R_\infty - R + a}{R_\infty} = \frac{|\overline{QB}|}{|\overline{QA}|} = \frac{\sin(\pi/2 - \varphi)}{\sin(\omega + \pi/2)} = \frac{\cos\varphi}{\cos\omega},$$
$$\frac{a}{R} = \frac{|\overline{PB}|}{|\overline{PC}|} = \frac{\sin(\pi/2 - \varphi')}{\sin(\pi/2 - \omega')} = \frac{\cos\varphi'}{\cos\omega},$$

where a denotes the length of the segment $\overline{PB}$, eliminating which we obtain

$$c\cos\varphi = (c-1)\cos\omega + \cos\varphi' \qquad (\text{recall } \mathrm{c} = \mathrm{R}_\infty/\mathrm{R}).$$

Approximating the cosines by second-order Taylor polynomials, we arrive at the following equations for $R_\infty \to R$ transitions:

$$\omega' = \omega; \qquad \varphi'^2 = c\varphi^2 - (c-1)\omega^2. \tag{2}$$

Now, if $c \gg 1$, then for most values of ω (unless $\omega \simeq \pm\varphi$), we have that φ' has order of magnitude $\sqrt{c}\varphi$, which is much larger than φ. More precisely, let us apply the map (2) to the almost-horizontal curve that has completed a series of consecutive collisions on the almost-flat arc. (φ is essentially constant and ω is evenly distributed on the interval $[-\varphi, \varphi]$). Then the image is a curve in the (ω', φ') coordinates that is much more extended vertically than horizontally: it consists of a sharply-increasing part (connecting the points $(-\varphi, \varphi)$ and $(0, \sqrt{c}\varphi)$) and a sharply-decreasing part (connecting the points $(0, \sqrt{c}\varphi)$ and (φ, φ)). For later reference, let us denote this curve by γ.

Note that the map (1) is expressed in terms of the (β, φ) coordinates, while the map (2) is expressed in terms of the (ω, φ) coordinates. Hence, before applying (2), the change of coordinates $(\beta, \varphi) \to (\omega, \varphi) = (\beta + \varphi, \varphi)$, and after applying (2), the change of coordinates $(\omega', \varphi') \to (\beta', \varphi') = (\omega' + \varphi', \varphi')$ are to be taken into account. However, as far as the geometry of curves is concerned, these coordinate changes can be regarded as additional applications of (1). In particular, it is enough to check that both parts of γ are good curves in the (ω', φ') coordinates. On the other hand, γ is far from being almost-horizontal. However, just after bypassing the corner point, the points of the curve start a long series of consecutive (sliding) bounces on the bottom (or top) arc. That is, the map (1) is applied many times, and as a result, the curve is strongly stretched along the horizontal direction. As a consequence, it can be partitioned into a large number of subcurves, the points of which reach the endpoint of the bottom arc simultaneously. Just before the $R \to R_\infty$ transition, all of these subcurves are almost horizontal.

We now turn to $R \to R_\infty$ transitions. Let us introduce the pre- and post-corner coordinates (ω, φ) and (ω', φ'), respectively. This time the quantities without primes correspond to the bottom (or top) arc, while the primed quantities correspond to the almost-flat arc. We obtain the same equations as above, with the role of φ and φ' interchanged:

$$\omega' = \omega, \qquad \varphi'^2 = \frac{1}{c}\varphi^2 + \left(1 - \frac{1}{c}\right)\omega^2. \tag{3}$$

Note that this time, even though φ' is smaller than φ, for most values of ω (unless $|\omega| \ll \varphi$) φ' has order of magnitude of φ. More precisely, let us apply the map (3) to the curve that has just completed a long series of consecutive bounces on the bottom (or the top) arc; that is, φ is essentially constant, while ω is evenly distributed on the interval $[-\varphi, \varphi]$. The image

is a curve in the (ω', φ') coordinates that has a decreasing and an increasing part: the former connects the points $(-\varphi, \varphi)$ and $(0, \frac{1}{\sqrt{c}}\varphi)$ with slope $\simeq -1$, while the latter connects the points $(0, \frac{1}{\sqrt{c}}\varphi)$ and (φ, φ) with slope $\simeq 1$; in particular, both parts are good curves. Now the points of this curve again start a series of consecutive bounces, this time on the almost-flat arc. By the time the next transition (this time an $R_\infty \to R$ transition) takes place, the curve has been subject to several applications of (1), which have stretched it in the horizontal direction, hence it consists of close-to-horizontal subcurves, the points of which bypass the corner point simultaneously. Then the whole argument can be iterated.

Let us make one more remark to avoid confusion. Of course, if we ran the dynamics backwards, we would need to apply the map (3) to the curve γ described above to obtain its *preimage* by an $R_\infty \to R$ transition. As (3) is the inverse of (2), we would obtain that the value of φ decreases by a factor $\frac{1}{\sqrt{c}}$ for most points of γ. However, γ is far from horizontal (actually, it is close to vertical) and the value of ω is far from being evenly distributed (actually, we have $|\omega| \ll \varphi$ for most points of γ). When investigating the forward dynamics, it is important that we apply both maps (3) and (2) to almost horizontal curves.

4.6. Summary

Summarising, for an overwhelming probability of phase points in our family (distributed smoothly along a good curve), the value of φ increases by a factor close to $\sqrt{c}$ at $R_\infty \to R$ transitions, and does not change drastically at $R \to R_\infty$ transitions. Overall, the value of φ thus increases on the average. Moreover, this increase is exponential in terms of the number of consecutive quasi-integrable (sliding) trajectory segments. Equivalently, we could say that the increase is exponential in terms of flow time, or in terms of the number of applications of the return map $\bar{T}^{\bar{c}}$. (Of course, the rate of increase in terms of the number of applications of the original map $T^{\bar{c}}$ can be arbitrary slow, as a single quasi-integrable segment may consist of an arbitrarily high number of bounces on the same arc).

Our argument above thus provides the following phenomenological description of the dynamics in generalised squashes with $b < 1$ and finite, but sufficiently large, c. The trajectory is subject to a strongly mixing dynamics in a large part of the phase space, away from the sliding region. From time to time, it makes excursions into the sliding region; however, on the average, it escapes from that region at an exponential speed. Note that these phenomena are completely analogous to what has been observed concerning consecutive bouncing trajectory segments in straight stadia, or consecutive diametrical segments of skewed stadia [10, 38, 11, 12]. Thus our observations provide strong support for our main conjecture.

These phenomena have been tested by convincing simulations, which can be reproduced by the reader using the program available at [39]. Note that on the phase portraits produced by this program, the configurational (horizontal) coordinate shown is k, rather than β, which should be kept in mind when comparing simulated trajectories with the above calculations.

5. Numerical evidence using Lyapunov-weighted dynamics

In this section, we look to support further our conjecture, by applying the powerful numerical method of Lyapunov-weighted dynamics to perform a more stringent search for elliptic islands in the two-dimensional (b, c) parameter space. The conjectured ergodic behaviour corresponds to the absence of such islands. Although no numerical method of this type can *prove* the absence of islands, we feel that the results presented here do provide support for the conjecture.

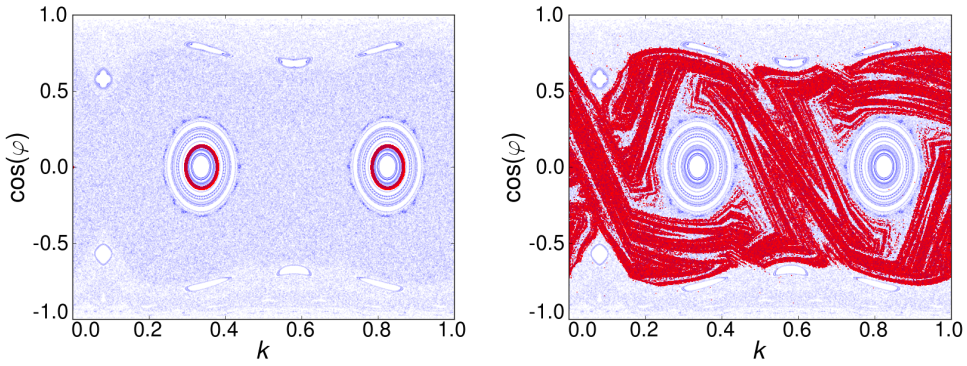

(a) $\alpha = -1$ (b) $\alpha = +1$

Figure 10. Results of applying LWD to a squash billiard with parameters $b = 0.6$ and $c = 1.6$, searching for both (a) regular and (b) chaotic regions. The thin (blue) points represent the evolution of randomly chosen initial conditions that evolve with the normal dynamics of the squash billiard, thus giving the standard representation of the phase space of the system. The (red) darker points show the superposition of the phase space locations during the last 100 collisions of 1000 walkers evolved under LWD for 10000 collisions.

The simplest method to search for islands consists of sampling from a grid of initial conditions in phase space and estimating the Lyapunov exponent or an equivalent indicator [40] for each one. However, this is unreliable and time-consuming, since the number of initial conditions needed to locate an island is inversely proportional to the area of the island in phase space, and we are interested in small islands.

A more powerful approach to locate regions of phase space with regular (i.e. non-chaotic) dynamics is the *Lyapunov-weighted dynamics* method (LWD), introduced in ref. [41]. The idea of this method is to evolve a population of walkers under a modified version of the dynamics, chosen so that the cloud of walkers spontaneously *concentrates* in regions of phase space which have a large (respectively small) Lyapunov exponent, according to whether a parameter α of the method is positive (respectively negative) [41].

To do so, each walker follows the underlying deterministic dynamics of the system under study, but perturbed by a small random noise of strength ε. Each walker also carries a tangent vector, which evolves under the tangent dynamics of the map. The local stretching factor of this tangent vector is calculated, as in the standard calculation of Lyapunov exponents, and walkers are killed or copied ("cloned") at a rate which is proportional to (α times) the stretching of their tangent vector [41]. This process can be shown to lead to the desired effect of the cloud of walkers "highlighting" the regions of chaotic or regular behaviour, depending on the value of α chosen [41]. Details of how the LWD method may be applied to billiard models will be discussed elsewhere.

Figure 10 illustrates the results of applying the LWD method to a generalised squash billiard, searching for both regular ($\alpha = -1$) and chaotic ($\alpha = +1$) dynamics. When $\alpha = -1$, the walkers concentrate in one of the elliptic islands of the phase space, whereas when α=1, the walkers instead stay in part of a chaotic component of the phase space, as shown in figure 10(b). In this case, there is in fact a partial barrier to transport in the phase space, visible around $\cos(\varphi) \simeq 0.7$ in figure 10. The LWD dynamics with $\alpha = +1$ nonetheless only sees part of this chaotic component.

Our approach is thus to exhaustively explore the (b,c) parameter space, looking for elliptic islands using LWD with $\alpha < 0$, in which case the walkers have a tendency to

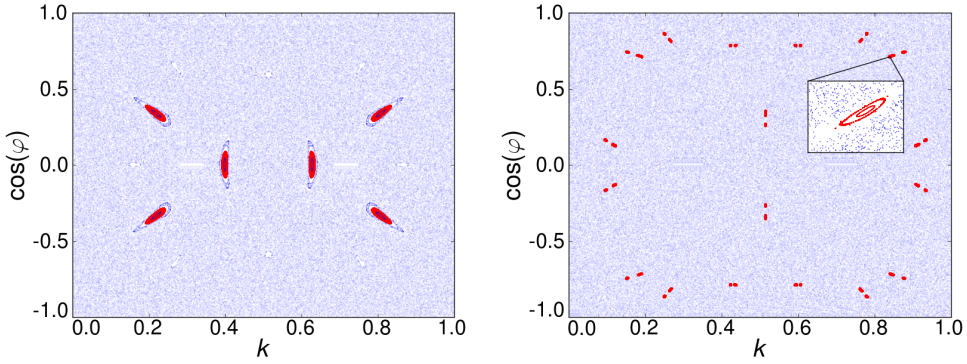

(a) $b = 0.1$, $c = 4$ (b) $b = 0.1$, $c = 6$

Figure 11. Results of applying LWD with $\alpha = -1$ to two squash billiards. The superposition of the last 100 collisions of 10000 walkers evolved under LWD for 10000 collisions is shown in (red) darker points on top of the phase space.

concentrate in the part of phase space which is "most stable", and thus to highlight any elliptic islands present. To exemplify the findings, figure 11(a) shows the results of applying LWD to a squash billiard with parameters $b = 0.1$ and $c = 4$. For these parameter values, there is an elliptic periodic trajectory of period 6, around which there is an elliptic island, but there is also a set of parabolic periodic orbits, corresponding to diametrical bouncing, since the lower circular arc is longer than a semi-circle, as discussed in section 2.2. When LWD is applied, the walkers concentrate exclusively around the elliptic island, with none trapped near the parabolic orbits, as shown in figure 11(a). This preference for the more stable islands is independent of both the size and the period of the island, as indicated in figure 11(b), where there are two islands of period 18, as well as parabolic bouncing orbits, for $c = 6$.

If, however, we now increase c further, to $c = 13$, then all of the walkers concentrate around the *parabolic* orbits, as shown in figure 12(a). This strongly suggests that there are no longer any elliptic islands in phase space, which would be more stable, and that the system is thus ergodic.

Applying LWD with $\alpha > 0$, that is, searching for the chaotic region, instead shows a complicated fractal structure, as shown in figure 12(b). This corresponds to the region of phase space where the rate of expansion is maximised. This region appears to fill phase space in a non-uniform way, avoiding the parabolic orbits. For comparison, figure 13 shows the results of applying LWD to a known ergodic system, the Bunimovich stadium. Similar behaviour is found as for the squash billiard, reinforcing ergodicity for the squash.

Nonetheless, it is possible that for the squash billiard, tiny elliptic islands in phase space still remain, whose area is below the threshold which may be detected using the LWD method. This threshold is the consequence of the noisy nature of the method, which we intend to explore in more detail elsewhere.

Figure 14 shows the qualitative behaviour observed over the two-dimensional (b,c) parameter space for $c < 50$, i.e. whether or not any elliptic islands were found with LWD for each pair (b,c). This picture provides strong evidence for our main conjecture, confirming that no islands are found by the method for c above a certain curve which is a function of b. The disappearance and reappearance of islands observed in the figure as c is increased for certain values of b is presumably related to the interplay of geometric destruction and complex series of period-doubling bifurcations [36] (see also section 3.3).

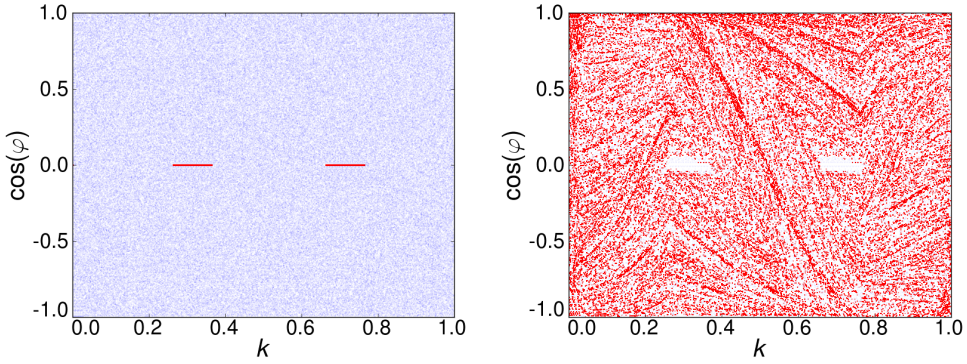

(a) $\alpha = -1$ (b) $\alpha = +1$

Figure 12. Results of applying LWD to a squash billiard with parameters $b = 0.1$ and $c = 13$. The superposition of the last 100 collisions of 1000 walkers evolved under LWD for 10000 collisions is shown in (red) darker points on top of the phase space.

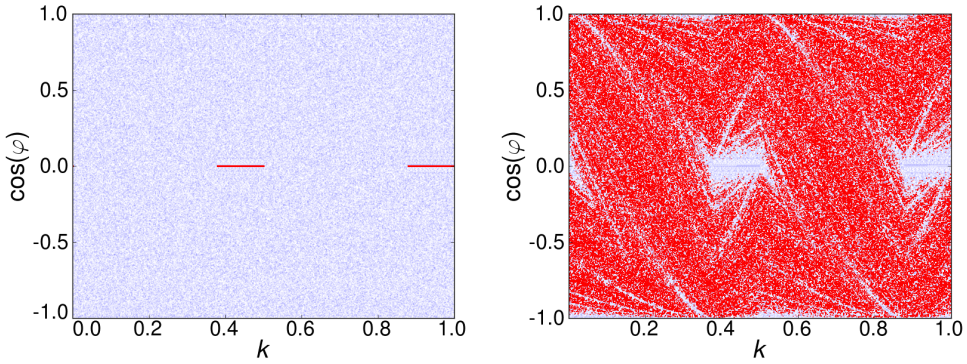

(a) $\alpha = -1$ (b) $\alpha = +1$

Figure 13. Results of applying LWD to an ergodic Bunimovich stadium. The superposition of the last 100 collisions of 1000 walkers evolved under LWD for 10000 collisions is shown in (red) darker points on top of the phase space.

We have also sampled even larger values of c at random, observing the same behaviour shown in figure 12, where the walkers concentrate around the parabolic orbits. As far as the LWD method allows us to exclude the existence of elliptic islands, we thus obtain further evidence pointing towards our main conjecture that the system is ergodic for $c > \hat{c}(b)$.

6. Conclusions

We have studied the dynamics of a two-parameter class of generalised squash billiards, which interpolates between completely integrable and completely chaotic dynamics. We have shown that the dynamical properties in the two-dimensional parameter plane are rather rich, involving a mixture of period-doubling behaviour reminiscent of smooth dynamics, and destruction of orbits caused by collisions with corners of the billiard table.

We have conjectured, based on heuristic arguments which we hope can be made rigorous, and extensive numerical simulations with both standard and Lyapunov-weighted methods, that

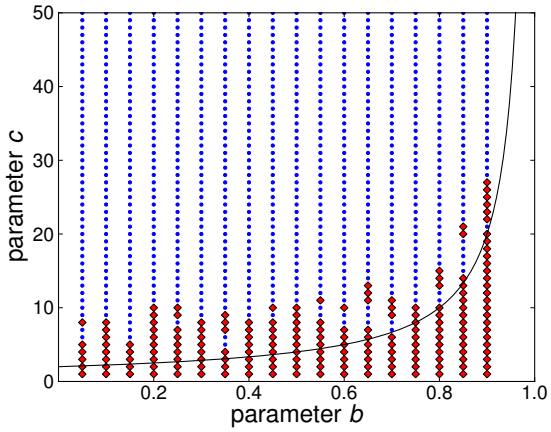

Figure 14. Parameter space of the generalised squash billiard. LWD with 1000 walkers evolving during 2000 collisions is applied to find regular regions ($\alpha = -1$). Pairs (b,c) that have elliptic islands found in this way are shown with (red) diamonds; pairs that do not have them are shown with (blue) points. The black continuous curve corresponds to $c_0(b)$.

all elliptic periodic points and their associated islands disappear for tables which are close enough to skewed stadia, thus giving a previously unknown class of ergodic convex billiards. It remains to characterize the parameter space in more detail, and prove the conjecture.

Acknowledgements

We thank the anonymous referees for their valuable comments which resulted in a significant improvement of the paper. PB acknowledges useful discussions with S. Troubetzkoy back in 2004, where the idea of studying generalised squashes originated. He also acknowledges financial support from the Bolyai Scholarship of the Hungarian Academy of Sciences, and OTKA (Hungarian National Fund for Scientific Research) grants F60206 and K71693. DPS acknowledges useful discussions with T. Gilbert and B. Krauskopf, and financial support from DGAPA-UNAM PAPIIT grant IN105209 and CONACYT grant CB101246.

Appendix A. Construction of generalised squash billiards

In this appendix, we sketch the geometric construction of generalised squash billiards. For fixed values of the parameters b and c, we must determine the radii and centers of the circular arcs that make up the table so that they satisfy the conditions of having common tangents at their points of intersection. To determine these quantities, we use the notation of Figure A1.

Fixing the parameter b determines the length of the top of the trapezium and the points P_1, P_2, P_3 and P_4. Since the table is symmetric about the vertical axis, it is only necessary to satisfy the tangent conditions for three arcs, since the right and left arcs have the same radii and their centers are reflected in the vertical axis.

The upper circular arc has radius r and center C_r, the lower arc has radius R and center C_R, and the right arc has radius R_∞ and center $C_{R\infty}$. Denote by M the midpoint of the segment joining P_1 and P_2, and by q a vector perpendicular to this segment.

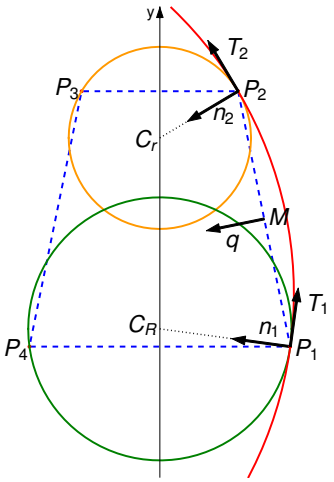

Figure A1. Geometry of generalised squash billiards. The trapezium is shown in (blue) dashed lines for a generic value of b. The different circular arcs are shown in different grey scales (colours).

By symmetry, C_r is on the y-axis, taking a suitable Cartesian coordinate system. Since $\|P_2 - C_r\| = r$, we have

$$C_r = \left(0, P_{2y} - \sqrt{r^2 - P_{2x}^2}\right). \tag{A.1}$$

This allows us to calculate the tangent to the upper circular arc T_2 at P_2, obtaining $T_2 = (C_r - P_2)_\perp$, where $v_\perp$ denotes a vector perpendicular to a given vector v.

Let us denote, furthermore, by n_2 the unit vector perpendicular to T_2. Since $C_{R_\infty} = P_2 + sn_2$, with $s \in \mathbb{R}$, we have $T_2 \cdot C_{R_\infty} = T_2 \cdot P_2$. Moreover, since C_{R_∞} is on the line through M with direction q, we find

$$C_{R_\infty} = M + t_2 q, \qquad \text{where } t_2 = \frac{T_2 \cdot P_2 - T_2 \cdot M}{T_2 \cdot q}. \tag{A.2}$$

With this we can calculate the tangent to the lower arc at the point P_1, obtaining $T_1 = (C_{R_\infty} - P_1)_\perp$.

Finally, $T_1 \cdot C_R = T_1 \cdot P_1$ and C_R is on the vertical axis, so

$$C_R = (0, t_1), \qquad \text{where } t_1 = \frac{T_1 \cdot P_1}{T_{1y}}. \tag{A.3}$$

These equations give us C_R and C_{R_∞} as a function of r, since T_2 is a function of r and T_1 is function of C_{R_∞}, which is also a function of r. Substituting these equations in the definition of the parameter c, we obtain

$$c = \frac{R_\infty}{R} = \frac{\|C_{R_\infty} - P_1\|}{\|C_R - P_2\|}, \tag{A.4}$$

giving an implicit equation for r in terms of b and c:

$$0 = f(r, b, c) = \|C_{R_\infty} - P_1\| - c\|C_R - P_2\|. \tag{A.5}$$

This equation may be solved numerically, for example by bisection, to find the value of r corresponding to given values of b and c. This can then be substituted back into equations (A.2) and (A.3) to get C_{R_∞} and C_R, and with this we obtain the radii of the other arcs:

$$R_\infty = \|C_{R_\infty} - P_1\|; \tag{A.6}$$

$$R = \|C_R - P_2\| . \tag{A.7}$$

Appendix B. Numerical methods

The dynamics of generalised squashes may be simulated by standard methods, namely finding the intersection of the particle trajectory with the circlular arcs forming the boundary. Periodic orbits may then be found by searching for iterates whose coordinates lie in a small neighborhood of a given initial condition.

The stability properties of a periodic orbit may be calculated using the tangent map of the dynamics, for which it is useful to take the (outgoing) local orthogonal section of the billiard map [2], rather than phase space coordinates. Coordinates just after collision are taken as the position $r \in Q$ and the velocity $v \in \mathbb{S}^1$; perturbations, up to linear order, are given by the coordinates (dr, dv), with both dr and dv perpendicular to the velocity v. Fix a phase point $x = (k, \varphi) \in M$, and denote its image under the dynamics as $x' = Tx = (k', \varphi') \in M$. Denote by K' the curvature of Γ at k', and by τ the free path (distance between k and k'). Then the image of a tangent vector (dr, dv) at x is the tangent vector (dr', dv') at x', given by [2]

$$\begin{pmatrix} dr' \\ dv' \end{pmatrix} = D \begin{pmatrix} dr \\ dv \end{pmatrix} = \begin{pmatrix} 1 & \tau \\ \frac{2K'}{\sin\varphi'} & 1 + \frac{2K'\tau}{\sin\varphi'} \end{pmatrix} \begin{pmatrix} dr \\ dv \end{pmatrix} . \tag{B.1}$$

The tangent map for a higher iterate may be calculated as the product of several such matrices. In particular if x is a periodic point of period p, i.e. $T^p x = x$, then it is possible to consider $D_p = D_x(T^p)$. In the local orthogonal section coordinates, the billiard map is area preserving, i.e. it has determinant 1. Thus the eigenvalue spectrum of D_p is characterized by the trace s of D_p: the orbit is hyperbolic, parabolic or elliptic, according as $|s| > 2$, $|s| = 2$ or $|s| < 2$, respectively. Hence s may be regarded as the *stability parameter* of the periodic orbit. Similarly, Lyapunov exponents of orbits may be estimated as the exponential growth rate with n of the trace of the product matrix giving the tangent map of the nth iterate.

References

[1] G. Benettin and J. M. Strelcyn. Numerical experiments on the free motion of a point mass moving in a plane convex region: Stochastic transition and entropy. *Phys. Rev. A*, 17:773–785, 1978.

[2] N. Chernov and R. Markarian. *Chaotic Billiards*. Amer. Math. Soc., 2006.

[3] M. Hénon and J. Wisdom. The Benettin–Strelcyn oval billiard revisited. *Physica D*, 8(2), 1983.

[4] L.A. Bunimovich. Mushrooms and other billiards with divided phase space. *Chaos*, 11, 2001.

[5] R. Markarian, S. Oliffson Khamporst, and S. Pinto de Carvalho. Chaotic properties of the elliptical stadium. *Comm. Math. Physics*, 174:661–679, 1996.

[6] C. Foltin. Billiards with positive topological entropy. *Nonlinearity*, 15:2053–2076, 2002.

[7] Holger R. Dullin, Peter H. Richter, and Andreas Wittek. A two-parameter study of the extent of chaos in a billiard system. *Chaos*, 6(1):43, 1996.

[8] L.A. Bunimovich. On ergodic properties of certain billiards. *Func. Anal. Appl.*, 8(3):254–255, 1974.

[9] Roberto Markarian. A lower bound for chaos on the elliptical stadium. *Physica D*, 115(4):189–202, 1998.

[10] N. Chernov and H.-K. Zhang. Billiards with polynomial mixing rates. *Nonlinearity*, 18:1527–1553, 2005.

[11] Péter Bálint and Sébastien Gouëzel. Limit theorems in the stadium billiard. *Comm. Math. Phys.*, 263(2):461–512, 2006.

[12] C. P. Dettmann and O. Georgiou. Survival probability for the stadium billiard. *Physica D*, 238:2395–2403, 2009.

[13] A. Hayli and Th. Dumont. Expériences numériques sur des billards C1 formés de quatre arcs de cercles. *Cel. Mech. Dyn. Astr.*, 38(1):23–66, 1986.

[14] Avram Hayli. Numerical exploration of a family of strictly convex billiards with boundary of class c^2. *J. Stat. Phys.*, 83:71–79, 1996. 10.1007/BF02183640.

[15] V Lopac, I Mrkonjic, and D Radic. Chaotic behavior in lemon-shaped billiards with elliptical and hyperbolic boundary arcs. *Phys. Rev. E*, 64, 2001.

[16] V Lopac, I Mrkonjic, and D Radic. Chaotic dynamics and orbit stability in the parabolic oval billiard. *Phys. Rev. E*, 66, 2002.

[17] V. Lopac, I. Mrkonjic, N. Pavin, and D. Radic. Chaotic dynamics of the elliptical stadium billiard in the full parameter space. *Physica D*, 217:88–101, 2006.

[18] V. Lopac and A. Simic. Chaotic properties of the truncated elliptical billiards. *Comm. Nonlin. Science Numer. Simul.*, pages –, 2010. In press.

[19] V. F. Lazutkin. On the existence of caustics for the billiard ball problem in a convex domain. *Math. USSR Izv.*, pages 185–215, 1973.

[20] R. Douady. *Applications du théorème des tores invariants. Thèse de 3ème cycle*. PhD thesis, Université Paris VII, 1982.

[21] A. Grigo. *Billiards and Statistical Mechanics*. PhD thesis, Georgia Institute of Technology, 2009.

[22] L. Bunimovich and A. Grigo. Focusing components in typical chaotic billiards should be absolutely focusing. *Comm. Math. Physics*, 293(1):127–143, 2010.

[23] L. Bussolari and M. Lenci. Hyperbolic billiards with nearly flat focusing boundaries, i. *Physica D*, 237(18):2272–2281, 2008.

[24] L. Bunimovich and G. del Magno. Track billiards. *Comm. Math. Physics*, 288(2):699–713, 2009.

[25] Holger R. Dullin and Arnd Bäcker. About ergodicity in the family of limaçon billiards. *Nonlinearity*, 14(6):1673, 2001.

[26] Serge Tabachnikov. *Billiards*. Société Mathématique de France, 1995.

[27] N. Chernov and H. K. Zhang. Regularity of Bunimovich's stadia. *Reg. Chaotic Dyn.*, 12:335–356, 2007.

[28] M. Wojtkowski. Principles for the design of billiards with nonvanishing Lyapunov exponents. *Comm. Math. Physics*, 105:391–414, 1986.

[29] R. Markarian. Billiards with Pesin region of measure one. *Comm. Math. Physics*, 118:87–97, 1988.

[30] V. Donnay. Using integrability to produce chaos: billiards with positive entropy. *Comm. Math. Physics*, 141:225–257, 1991.

[31] L. A. Bunimovich. On absolutely focusing mirrors. In U. Krengel et al., editor, *Ergodic Theory and related topics, III*, number 1514 in Lecture Notes in Mathematics, pages 62–82. Springer-Verlag, 1992.

[32] D. Szász. On the K-property of some planar hyperbolic billiards. *Comm. Math. Physics*, 145:595–604, 1992.

[33] R. Markarian. New ergodic billiards: exact results. *Nonlinearity*, pages 819–841, 1993.

[34] M. Di Bernardo, C.J. Budd, A.R. Champneys, and P. Kowalczyk. *Piecewise-Smooth Dynamical Systems: Theory and Applications*, volume 163 of *Applied Mathematical Sciences*. Springer Verlag, 2008.

[35] D.J.W. Simpson and J.D. Meiss. Simultaneous border-collision and period-doubling bifurcations. *Chaos*, 19:033146, 2009.

[36] R. S. MacKay. *Renormalisation in Area-Preserving Maps*, volume 6 of *Advanced Series in Nonliear Dynamics*. World Scientific, 1993.

[37] A. Arroyo, R. Markarian, and D. P. Sanders. Bifurcations of periodic and chaotic attractors in pinball billiards with focusing boundaries. *Nonlinearity*, 22(7):1499–1522, 2009.

[38] N. Chernov and H.-K. Zhang. Improved estimates for correlations in billiards. *Comm. Math. Phys.*, 277(2):305–321, 2008.

[39] Miklós Halász. Computer software freely available at `http://www.renyi.hu/~bp/miki/program/readme.html`.

[40] Zs. Sándor, B. Érdi, A. Széll, and B. Funk. The relative Lyapunov indicator: an efficient method of chaos detection. *Celest. Mech. Dyn. Astron.*, 90(2):127–138, 2004.

[41] J. Tailleur and J. Kurchan. Probing rare physical trajectories with Lyapunov Weighted Dynamics. *Nature Phys.*, **3**:203–207, 2007. See also the Supplementary Information.